WATER RESOURCES RESEARCH, VOL. 44, W12416, doi:10.1029/2008WR007014, 2008

Temporal moments in geoelectrical monitoring of salt tracer experiments

Davina Pollock[1] and Olaf A. Cirpka[1,2]

Received 20 March 2008; revised 20 August 2008; accepted 3 September 2008; published 13 December 2008.

[1] Monitoring of salt tracer experiments by electrical resistivity tomography (ERT) has been shown to be a valuable tool for characterizing the hydraulics of an aquifer, but efficient approaches of determining the spatial hydraulic conductivity distribution from ERT data are still missing. Standard inversion of ERT data obtained during salt tracer tests may even lead to estimates of the concentration distribution that are in contradiction to flow and transport of conservative compounds in porous media. In order to avoid nonphysical behavior, we consider the governing equations of groundwater flow, solute transport, and geoelectrics as a coupled system. While the tracer passes through the part of the domain that is sensitive for a particular electrode configuration, the measured electrical potential differences are perturbed. We characterize these perturbations by their temporal moments and relate them to the temporal moments of concentration, which themselves depend on hydraulic conductivity. We present temporal moment-generating equations leading from the hydraulic conductivity field via heads and velocities to the temporal moments of concentration and electrical potential perturbations. The approach makes use of a linearized version of the Poisson equation. On the basis of this system of coupled steady state equations, we compute the sensitivity of electrical potential perturbations with respect to the log hydraulic conductivity distribution by the continuous adjoint state method for coupled systems. For demonstration, we simulate salt tracer experiments in a virtual quasi-two-dimensional sandbox, monitored by ERT. We show that the ratio of the first over the zeroth temporal moment of potential perturbation is less affected by the linearization of the Poisson equation than the zeroth and first moments themselves. Thus, it appears recommendable to use the ratio of first to zeroth moments also as data in inversion. We compare sensitivity patterns resulting from different electrode configurations. The methods of forward simulations and sensitivity calculations presented in this paper can be combined with any inverse kernel to develop a complete inverse model. Altogether, using temporal moments of potential perturbation appears promising for fully coupled hydrogeophysical inversion of ERT surveys during salt tracer tests.

Citation: Pollock, D., and O. A. Cirpka (2008), Temporal moments in geoelectrical monitoring of salt tracer experiments, *Water Resour. Res.*, *44*, W12416, doi:10.1029/2008WR007014.

1. Introduction

[2] The estimation of hydraulic conductivity in heterogeneous aquifers is a remaining challenge of subsurface hydrology. The variability of hydraulic conductivity has a major impact on solute transport, so that assessing an effective mean value in a formation is insufficient. Various field methods exist for estimating hydraulic conductivity, most of which require the installation of monitoring wells (e.g., pumping tests, flowmeter tests and monitoring of tracer tests in wells). The costs of installing monitoring wells limit the number of observation points, often leading to an insufficient resolution [e.g., *Li et al.*, 2007, 2008]. In hydrogeophysics, nonintrusive geophysical methods are applied to hydrological problems [see *Rubin and Hubbard*, 2005]. Standard geophysical surveys lead to the distribution of seismic, gravimetric, electric, magnetic or electromagnetic properties in the subsurface. This enables reconstructing the subsurface structure, but does not provide much information regarding its hydraulic properties. Recently, *Slater* [2007] presented a review on the integration of geophysical and hydrological measurements in hydrogeological contexts. Rather than using geophysical exploration techniques for the identification of the subsurface structure, they may also be used to monitor hydraulic experiments (e.g., infiltration experiments [*Daily et al.*, 1992], pumping tests [*Sloan et al.*, 2007; *Rizzo et al.*, 2004], and tracer tests [*Binley et al.*, 1996]), where the geophysical signal reflects the response to the hydraulic stress applied in the experiment.

[3] A particularly promising technique is the monitoring of salt tracer experiments by electrical resistivity tomography (ERT), with which the values of electrical conductivity and subsequently of concentration can be inferred [*Binley et*

[1]Eawag, Swiss Federal Institute of Aquatic Science and Technology, Dübendorf, Switzerland.
[2]Now at Center of Applied Geosciences, University of Tübingen, Tübingen, Germany.

0043-1397/08/2008WR007014$09.00

al., 1996, 2002; *Slater et al.*, 2000; *Kemna et al.*, 2002; *Vanderborght et al.*, 2005; *Singha and Gorelick*, 2005]. Further processing the concentration distribution has been suggested in order to identify the spatial distribution of hydraulic properties [e.g., *Kemna et al.*, 2002; *Vanderborght et al.*, 2005]. In the cited studies, the geoelectrical inversion was performed by standard ERT inversion techniques, mostly on the basis of Tikhonov regularization, and the thus reconstructed images of electrical conductivity were subsequently analyzed. *Singha and Gorelick* [2005], for example, computed spatial moments of concentration from ERT surveys, observing that only about 50% of the total injected solute mass (described by the zeroth moment) was recovered by the inversion. This nonphysical behavior results from decoupled ERT inversion lacking constraints from flow and transport.

[4] The ultimate goal of a tracer test is the identification of the distribution of hydraulic conductivity, which is a material property. Toward this goal, imaging a tracer plume and analyzing its spatial moments could only be a first step. In theory, the hydraulic conductivity distribution could be inferred from taking the concentration images of multiple ERT surveys performed at different times as point-like measurements. Considering that a three-dimensional ERT inversion results in tens of thousands of electrical conductivity values, and that a time series may be made of hundreds of time points, the amount of data to be handled appears overwhelming. Moreover, the concentration estimates from ERT inversion are uncertain and correlated, so that in subsequent analysis the point estimates of concentration must not be treated as independent measurements. Not very surprisingly, the actual estimation of hydraulic conductivity from time-lapse ERT surveys during tracer tests is still missing.

[5] In conclusion, there is a clear need for efficient analysis tools for geoelectrical monitoring of salt tracer tests in which flow, solute transport, and geoelectrical surveying are considered as a coupled system. The development of such methods consists of the following four components: (1) an appropriate choice of what is treated as measurement for inversion, (2) an efficient forward model predicting the measured quantity from hydraulic conductivity, other material properties, and boundary conditions, (3) an efficient method of computing the sensitivity of the measured quantities with respect to hydraulic conductivity, and (4) an inverse kernel. This paper deals with the first three points. The key of our approach is to consider the temporal moments of electrical potential perturbations obtained during time-lapse ERT surveying of salt tracer experiments. We show how the temporal moments of the measured electrical signals can directly be related to the temporal moments of concentration throughout the domain. Temporal moments of concentration measurements have already successfully been used to infer the hydraulic conductivity distribution [*Harvey and Gorelick*, 1995; *Cirpka and Kitanidis*, 2000; *James et al.*, 2000; *Nowak and Cirpka*, 2006]. Thus, we propose extending these existing methods to include geoelectrical observation by ERT.

[6] The current contribution differs from the recent studies of *Singha et al.* [2007] and *Day Lewis and Singha* [2008] who also considered temporal moments of ERT data. The latter authors considered formations exhibiting dual-porosity behavior. They argued that temporal moments observed by ERT reflect the moments of the total concentration, that is, the solute mass in both the mobile and immobile pore space per bulk volume. These moments were compared to those obtained by measuring the solute concentration in samples, which are exclusively extracted from the mobile pore space. In the present study, we do not account for dual-porosity behavior although such extensions would be possible. Also, we do not rely on independent concentration measurements based on sampling. In contrast to *Singha et al.* [2007] and *Day Lewis and Singha* [2008], we relate the hydraulic conductivity field, rather than parameters describing mobile-immobile mass transfer kinetics, to the temporal moments of ERT data.

[7] This paper is organized as follows: In section 2, we review the governing equations of groundwater flow, solute transport, and direct current geoelectrics. In section 3, we present the temporal moment-generating equations for concentration and electrical potential. In section 4, we show how the sensitivity of electrical potential moments with respect to hydraulic conductivity can be computed without explicit evaluation of sensitivities involving intermediate quantities. In section 6, we present an artificial two-dimensional test case, which is motivated by a planned intermediate-scale sandbox experiment where electrodes extend through the entire width of the box. We analyze the validity of underlying assumptions and discuss the sensitivity of different electrode arrays.

2. Governing Equations

[8] In this section, we review the governing equations describing groundwater flow and transport, and the effect of tracer injection on electrical conductivity and electrical potential during geoelectrical surveying.

[9] We assume steady state groundwater flow without internal sinks or sources, leading to

$$\nabla \cdot (K \nabla h) = 0 \tag{1}$$

subject to the boundary conditions

$$h = h_0 \text{ at } \Gamma_D \tag{2}$$

$$\mathbf{n} \cdot (K \nabla h) = q_0 \text{ at } \Gamma_N \tag{3}$$

$$\mathbf{n} \cdot (K \nabla h) = \lambda (h \quad h_{ref}) \text{ at } \Gamma_C \tag{4}$$

in which K is the hydraulic conductivity, here assumed isotropic, h is the hydraulic head and $\mathbf{n}$ denotes the unit vector normal to the boundary Γ. The latter is subdivided into a Dirichlet boundary, Γ_D, with fixed head h_0, a Neumann boundary, Γ_N, with fixed normal flux q_0 (in many cases zero), and a Cauchy boundary, Γ_C, with a normal flux linearly depending on the head; the proportionality coefficient λ is known as leakage coefficient, and h_{ref} is a known reference head. The specific discharge $\mathbf{q}$ follows Darcy's law:

$$\mathbf{q} = \quad K \nabla h \tag{5}$$

[10] The concentration of a tracer introduced into the aquifer through an inflow boundary Γ_{in} is commonly described by the advection-dispersion equation

$$\theta\frac{\partial c}{\partial t}+\mathbf{q}\cdot\nabla c \quad \nabla\cdot(\theta\mathbf{D}\nabla c)=0 \tag{6}$$

subject to the initial and boundary conditions:

$$c=0\ \forall\ \mathbf{x}\ \text{at}\ t=0 \tag{7}$$

$$c(t,\mathbf{x})=c_0(t,\mathbf{x})\ \text{at}\ \Gamma_{\text{in}} \tag{8}$$

$$\mathbf{n}\cdot(\mathbf{D}\nabla c)=0\ \text{at}\ \Gamma_{\text{no flow}}\cup\Gamma_{\text{out}}\forall t \tag{9}$$

where θ is the porosity, $\mathbf{D}$ is the dispersion tensor, $c_0(t, \mathbf{x})$ is a known, time- and coordinate-dependent concentration along the inflow boundary, and the boundary $\Gamma = \Gamma_{\text{in}} \cup \Gamma_{\text{no flow}} \cup \Gamma_{\text{out}}$ is now subdivided into an inflow, a no-flow, and an outflow section. Unlike *Singha et al.* [2007], we assume that solute storage in an immobile fraction of the pore space can be neglected, or is sufficiently accounted for in the dispersion term. Thus, we do not discriminate between concentrations and associated contributions to bulk electrical conductivity in mobile and immobile pore fractions. For the hydrodynamic dispersion tensor, we assume the standard linear dependence on velocity:

$$\theta\mathbf{D}=\frac{\mathbf{q}\otimes\mathbf{q}}{\|\mathbf{q}\|}(\alpha_l \quad \alpha_t)+\mathbf{I}(\|\mathbf{q}\|\alpha_t+\theta D_m) \tag{10}$$

in which $\otimes$ denotes a matrix product, α_l and α_t are longitudinal and transverse dispersivities, respectively, $\mathbf{I}$ is the identity matrix, and D_m is the pore diffusion coefficient.

[11] The bulk electrical conductivity field $\sigma(t, \mathbf{x})$ in an aquifer can be expressed as the sum of the background conductivity σ_0, constant through time and independent of concentration, and a concentration-dependent term:

$$\sigma(t,\mathbf{x})=\sigma_0(\mathbf{x})+\kappa c(t,\mathbf{x}) \tag{11}$$

where κ is a proportionality constant which can be derived from Archie's law [*Archie*, 1942] and $c(t, \mathbf{x})$ indicates the concentration of the tracer. In the following we denote the concentration-dependent term as the perturbation of electrical conductivity σ':

$$\sigma'(t,\mathbf{x})=\kappa c(t,\mathbf{x}) \tag{12}$$

which causes a perturbation of the electrical potential. We consider a direct current geoelectrical survey, in which the current I is injected into the subsurface at location $\mathbf{x}_i$ and extracted at location $\mathbf{x}_o$. The electrical potential φ follows the Poisson equation:

$$\nabla\cdot(\sigma\nabla\varphi)=I(\delta(\mathbf{x}\quad\mathbf{x}_o)\quad\delta(\mathbf{x}\quad\mathbf{x}_i)) \tag{13}$$

[12] The application presented in section 6 mimics a quasi-two-dimensional sandbox experiment in which all sides are electrically insulated, resulting in a no-current boundary condition along the entire boundary:

$$\mathbf{n}\cdot\nabla\varphi=0\ \text{at}\ \Gamma_{\text{n.c.}} \tag{14}$$

in which $\delta()$ is the Dirac delta function, and $\Gamma_{\text{n.c.}}$ is the no-current boundary.

[13] In a field experiment, the land surface acts as an electrical insulator, whereas electrical currents extend beyond all other boundaries of the hydraulic domain. A common way of coping with a semi-infinite medium in simulations is to extend the domain used for geoelectrical simulations far beyond the actual area of interest. Then, applying a no-current boundary of the simulation would not cause a major bias in the area of interest. As an alternative, a mixed boundary condition may be applied, particularly at the bottom boundary [*Dey and Morrison*, 1979]:

$$\mathbf{n}\cdot\nabla\varphi+\beta\varphi=\gamma\ \text{at}\ \Gamma_{\text{mix}} \tag{15}$$

in which the coefficients β and γ are chosen such that the Poisson equation for uniform coefficients in a semi-infinite domain is met at the boundary. In such a framework the boundary of the domain is subdivided into the no-current boundary $\Gamma_{\text{n.c.}}$ and the mixed-condition boundary Γ_{mix}.

[14] In geoelectrical inversion, the electrical conductivity σ is inferred from measurements of electrical potential. In general, we consider the potential difference $\Delta\varphi$ between two measurement locations $\mathbf{x}_{m_1}$ and $\mathbf{x}_{m_2}$:

$$\begin{aligned}\Delta\varphi(t)&=\varphi(t,\mathbf{x}_{m_1})\quad\varphi(t,\mathbf{x}_{m_2})\\&=\int_\Omega\varphi(t,\mathbf{x})(\delta(\mathbf{x}\quad\mathbf{x}_{m_1})\quad\delta(\mathbf{x}\quad\mathbf{x}_{m_2}))d\mathbf{x}\end{aligned} \tag{16}$$

in which Ω is the entire domain. In the Poisson equation, equation (13), the relationship between electrical potential φ and electrical conductivity σ is nonlinear. As we will see in section 3, the derivation of temporal moment-generating equations requires linear relationships. Thus, we linearize the Poisson equation about the background electrical conductivity σ_0. To this means, the potential φ may be expressed as the sum of the base potential φ_0, observed in the absence of the tracer, and the potential perturbation φ', induced by the presence of the tracer:

$$\varphi=\varphi_0+\varphi' \tag{17}$$

[15] Substituting equation (17) into equation (13), subtracting the Poisson equation in the absence of the tracer, and dropping products of perturbations yields the Poisson equation linearized about σ_0:

$$\nabla\cdot(\sigma_0\nabla\varphi')=\quad\nabla\cdot(\sigma'\nabla\varphi_0) \tag{18}$$

subject to

$$\mathbf{n}\cdot\nabla\varphi'=0\ \text{at}\ \Gamma_{\text{n.c.}} \tag{19}$$

$$\mathbf{n}\cdot\nabla\varphi'+\beta\varphi'=0\ \text{at}\ \Gamma_{\text{mix}} \tag{20}$$

Substituting equation (12) into equation (18) gives

$$\nabla \cdot (\sigma_0 \nabla \varphi') = \quad \nabla \cdot (\kappa c \nabla \varphi_0) \tag{21}$$

[16] Equation (21) approximately describes how the concentration distribution $c(t, \mathbf{x})$ causes perturbations of electrical potential φ'. It depends on the location and strength of current injection and extraction via the distribution of the base potential φ_0. In the course of a tracer experiment, the solute plume passes through the domain, causing measured electrical potential differences $\Delta\varphi'(t)$ for a given electrode configuration. In the initial state and in the large-time limit, $\Delta\varphi'(t)$ is zero. Equation (21) is only an approximation because it is based on the linearized Poisson equation of equation (18), where the product of perturbations $\nabla \cdot (\kappa c \nabla \varphi')$ has been dropped on the right-hand side. Strictly speaking, this approximation is only valid for $\kappa c \ll \sigma_0$, which is in contrast to achieving a well detectable potential signal caused by the presence of the tracer. In section 6.2, we discuss the effects of linearization on measurable potential differences during a salt tracer test with realistic electrical conductivity contrasts.

3. Temporal Moments

[17] We now introduce temporal moments of concentration $c(t, \mathbf{x})$ and of electrical potential perturbations $\varphi'(t, \mathbf{x})$. The kth raw temporal moment of concentration $m_k^c(\mathbf{x})$ is defined as

$$m_k^c(\mathbf{x}) = \int_0^\infty t^k c(t, \mathbf{x}) dt \tag{22}$$

[18] For all temporal moments to be finite, the concentration must drop at least exponentially in the large-time limit [e.g., *Harvey and Gorelick*, 1995]. The latter condition is met for typical cases of tracer injection over a finite time. In case of continuous tracer injection with uniform inflow concentration (step-input problem), it is possible to compute truncated moments in which the upper bound of the integral in equation (22) is finite. From the asymptotic large-time value of the step input problem and the truncated moments one can compute the corresponding moments for a pulse-like injection [e.g., *Jose and Cirpka*, 2004; *Li et al.*, 2005].

[19] The zeroth and first temporal moments of concentration represent the integral of the breakthrough curve (total mass of solute passing through the measurement volume divided by the discharge) and the mean arrival time of the solute times the zeroth moment. The second moment contains information about the spread. Here we consider only the zeroth and first moment, and the ratio of these quantities (i.e., the mean arrival time).

[20] In the same way, we can compute the kth temporal moment of the perturbations of electrical potential:

$$m_k^{\varphi'}(\mathbf{x}) = \int_0^\infty t^k \varphi'(t, \mathbf{x}) dt \tag{23}$$

[21] For the perturbation of potential differences $\Delta\varphi'(t) = \varphi'(t, \mathbf{x}_{m_1}) - \varphi'(t, \mathbf{x}_{m_2})$, in which $\mathbf{x}_{m_1}$ and $\mathbf{x}_{m_2}$ are the two locations of electrical potential measurements, the raw temporal moments are defined as

$$m_k^{\Delta\varphi'} = \int_0^\infty t^k (\varphi'(t, \mathbf{x}_{m_1}) \quad \varphi'(t, \mathbf{x}_{m_2})) dt = m_k^{\varphi'}(\mathbf{x}_{m_1}) \quad m_k^{\varphi'}(\mathbf{x}_{m_2}) \tag{24}$$

[22] We multiply the advection-dispersion equation, equation (6), the linearized Poisson equation, equation (21), and their boundary conditions by t^k, integrate over time and apply integration by parts, to obtain the following temporal moment-generating equations for concentration [*Harvey and Gorelick*, 1995] and electrical potential perturbation, respectively:

$$\mathbf{q} \cdot \nabla m_k^c \quad \nabla \cdot \left(\theta \mathbf{D} \nabla m_k^c\right) = k\theta m_{k-1}^c \tag{25}$$

subject to

$$m_k^c = m_k^{c_0} \text{ at } \Gamma_{\text{in}} \tag{26}$$

$$\mathbf{n} \cdot \left(\mathbf{D} \nabla m_k^c\right) = 0 \text{ at } \Gamma_{\text{no flow}} \cup \Gamma_{\text{out}} \tag{27}$$

and

$$\nabla \cdot \left(\sigma_0 \nabla m_k^{\varphi'}\right) = \quad \nabla \cdot \left(\kappa m_k^c \nabla \varphi_0\right) \tag{28}$$

subject to

$$\mathbf{n} \cdot \nabla m_k^{\varphi'} = 0 \text{ at } \Gamma_{\text{n.c.}} \tag{29}$$

$$\mathbf{n} \cdot \nabla m_k^{\varphi'} + \beta m_k^{\varphi'} = 0 \text{ at } \Gamma_{\text{mix}} \tag{30}$$

[23] The moment-generating equation for concentration, equation (25), is formally identical to the advection-dispersion equation in steady state, implying that temporal moments of concentration can directly be computed without solving the transient transport equation. The moment-generating equation for potential perturbation, equation (28), does not show a time dependency either and can also be solved directly without having to compute the potential perturbation at each time step.

4. Sensitivities of Electrical Potential Moments on Hydraulic Conductivity

[24] The sensitivity of a particular measurement on a parameter of interest is the corresponding partial derivative. Since hydraulic conductivity is a spatial variable, we are interested in sensitivity fields, quantifying how the model outcome of a particular measurement depends in the linear limit on hydraulic conductivity throughout the domain. Sensitivity analysis is an important step in model calibration and experimental design. In our application, a measurement is defined as a temporal moment of electrical potential perturbation for given pairs of current and potential electrodes. If such a measurement is not sensitive to hydraulic conductivity in a certain part of the domain, it is impossible to infer the value of the latter from the former. In an optimal

experimental design, the sensitivity patterns of the various measurements differ as much as possible, and hydraulic conductivity at each location in the domain is sensitive to at least one measurement.

[25] In the following, we consider that the log hydraulic conductivity field $Y(\mathbf{x})$ is discretized in subvolumes with uniform value, leading to a parameter vector $\mathbf{Y}$. The size of a subvolume equals that of a Finite Element in the numerical evaluation of the governing equations. Then, the sensitivity matrix is the matrix of partial derivatives of all measurements with respect to all parameters. The most simple method to calculate sensitivities is by direct numerical differentiation, where the forward problem is successively repeated, each time with small variations of a single parameter. The sensitivity matrix is then computed as the ratio of the variation of all measured quantities over the variation of each parameter. In an application with n unknowns and m measurements, it is necessary to solve $n + 1$ problems to compute the full sensitivity matrix. With one parameter per Finite Element, this approach becomes exceedingly costly for high spatial resolutions. Also, the higher the spatial resolution of the log hydraulic conductivity field, the smaller is the effect of varying its value in a single element. Therefore, sensitivities obtained by direct numerical differentiation in highly resolved domains may strongly be affected by slight inaccuracies of the numerical methods used to solve the systems of partial differential equations.

[26] A more efficient method of computing sensitivities is the continuous adjoint state method for coupled systems by *Sun and Yeh* [1990], which we apply in the following. For each observation, we have to solve a set of adjoint problems similar to the forward problem, which in case of underdetermined problems provides a large gain in computational costs compared to the calculation by direct numerical differentiation. The procedure is practically identical to the one used by *Cirpka and Kitanidis* [2000] and *Nowak and Cirpka* [2006] to compute the sensitivities of the moments of concentration with respect to the log hydraulic conductivity, except for the addition of electrical potentials.

[27] For a given measurement, we denote the adjoint states for hydraulic head, zeroth concentration moment, first concentration moment and electrical potential by a_h, a_0, a_1 and a_φ, respectively. As a first step, we solve the adjoint linearized Poisson equation to compute the adjoint state of electrical potential:

$$\nabla \cdot \left(\sigma_0 \nabla a_\varphi\right) = \delta(\mathbf{x} \quad \mathbf{x}_{m_2}) \quad \delta(\mathbf{x} \quad \mathbf{x}_{m_1}) \tag{31}$$

subject to

$$\mathbf{n} \cdot \nabla a_\varphi = 0 \text{ at } \Gamma_{\text{n.c.}} \tag{32}$$

$$\mathbf{n} \cdot \nabla a_\varphi + \beta a_\varphi = 0 \text{ at } \Gamma_{\text{mix}} \tag{33}$$

where $\mathbf{x}_{m_1}$ and $\mathbf{x}_{m_2}$ are the two measurement locations.

[28] For first-moment measurements, the equation for the adjoint state of the first moment of concentration has to be solved next:

$$\mathbf{q} \cdot \nabla a_1 \quad \nabla \cdot (\theta \mathbf{D} \nabla a_1) = \quad \nabla a_\varphi \cdot \nabla \varphi_0 \kappa \tag{34}$$

subject to

$$a_1 = 0 \text{ at } \Gamma_{\text{out}} \tag{35}$$

$$\mathbf{n} \cdot (\theta \mathbf{D} \nabla a_1) = 0 \text{ at } \Gamma_{\text{in}} \cup \Gamma_{\text{no flow}} \tag{36}$$

[29] In case of a first-moment measurement, the adjoint state of the first concentration moment, a_1, is needed to calculate the adjoint state of the zeroth concentration moment, a_0, which is given by

$$\mathbf{q} \cdot \nabla a_0 \quad \nabla \cdot (\theta \mathbf{D} \nabla a_0) = a_1 \theta \delta_{k1} \quad \nabla a_\varphi \cdot \nabla \varphi_0 \kappa \delta_{k0} \tag{37}$$

subject to

$$a_0 = 0 \text{ at } \Gamma_{\text{out}} \tag{38}$$

$$\mathbf{n} \cdot (\theta \mathbf{D} \nabla a_0) = 0 \text{ at } \Gamma_{\text{in}} \cup \Gamma_{\text{no flow}} \tag{39}$$

where $k = 0$ for a zeroth-moment measurement and $k = 1$ for a first-moment measurement. The Kronecker delta δ_{ij} equals one if both indices are identical and zero otherwise. In case of a first-moment measurement, therefore, the adjoint state of the first concentration moment, a_1, appears on the right-hand side of the partial differential equation for a_0 as a source-sink term. In case of a zeroth-moment measurement, the adjoint state of the first moment is not needed, and only the second source-sink term of equation (37) has to be considered. From this equation it is clear that a_0 is not the same for measurements of the first and the zeroth moments.

[30] The last adjoint variable to be computed is the adjoint state of the hydraulic head, a_h, which follows the adjoint groundwater flow equation:

$$\nabla \cdot (K \nabla a_h) = \quad \nabla \cdot \left(a_1 K \nabla m_1^c\right) \quad \nabla \cdot \left(a_0 K \nabla m_0^c\right) \tag{40}$$

subject to

$$a_h = 0 \text{ at } \Gamma_{\text{D}} \tag{41}$$

$$\mathbf{n} \cdot (K \nabla a_h) = \quad a_1 \mathbf{n} \cdot \nabla m_1^c K \quad a_0 \mathbf{n} \cdot \nabla m_0^c K \text{ at } \Gamma_{\text{N}} \tag{42}$$

$$\mathbf{n} \cdot (K \nabla a_h) = \quad a_1 \mathbf{n} \cdot \nabla m_1^c K \quad a_0 \mathbf{n} \cdot \nabla m_0^c K \quad \lambda a_h \text{ at } \Gamma_{\text{C}} \tag{43}$$

where, in case of a zeroth-moment measurement, the first term on the right-hand side of equation (40) equals zero and a_0 is different for a zeroth- and first-moment measurement, respectively.

[31] Finally, the sensitivity of the first temporal moment of potential perturbation $\Delta\varphi'$ with respect to a particular log hydraulic conductivity value Y_λ is

$$\frac{\partial m_1^{\Delta\varphi'}}{\partial Y_\lambda} = \quad \int_{V_\lambda} \left(\nabla a_h \cdot \nabla h K + a_0 K \nabla h \cdot \nabla m_0^c + a_1 K \nabla h \cdot \nabla m_1^c\right) dV \tag{44}$$

where V_λ is a subvolume with uniform conductivity Y_λ.

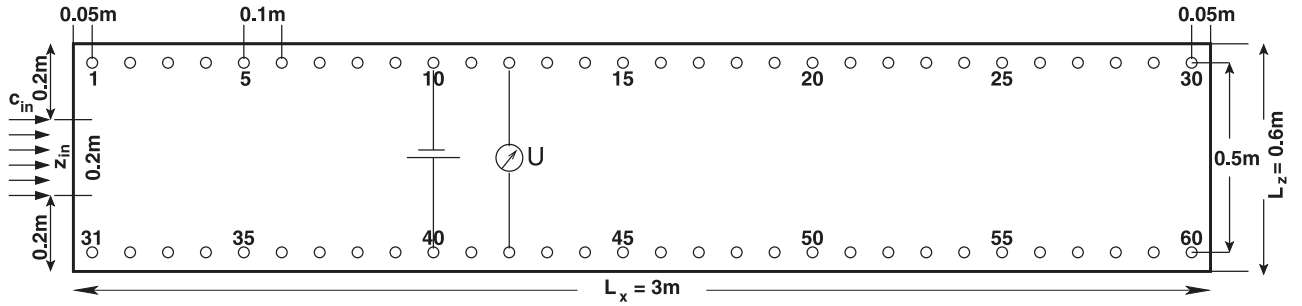

Figure 1. Schematic setup of the sandbox. The circles indicate the location of the electrodes, numbered 1 to 60. The electrode configuration indicated here is the one used in section 6.2 to test the validity of the linearization.

[32] Analogously, the sensitivity of the zeroth temporal moment of potential perturbation with respect to log hydraulic conductivity becomes (this time using the adjoint states obtained for zeroth-moment measurements)

$$\frac{\partial m_0^{\Delta\varphi'}}{\partial Y_\lambda} = \int_{V_\lambda} \left(\nabla a_h \cdot \nabla hK + a_0 K \nabla h \cdot \nabla m_0^c\right) dV \qquad (45)$$

[33] To obtain the sensitivity of the mean arrival time of the potential perturbation with respect to log hydraulic conductivity, we apply the chain rule of differentiation:

$$\frac{\partial}{\partial Y_\lambda}\left(\frac{m_1^{\Delta\varphi'}}{m_0^{\Delta\varphi'}}\right) = \frac{1}{m_0^{\Delta\varphi'}}\frac{\partial m_1^{\Delta\varphi'}}{\partial Y_\lambda} \quad \frac{m_1^{\Delta\varphi'}}{\left(m_0^{\Delta\varphi'}\right)^2}\frac{\partial m_0^{\Delta\varphi'}}{\partial Y_\lambda} \qquad (46)$$

[34] As has already been pointed out by *Sun and Yeh* [1990] and *Cirpka and Kitanidis* [2000], among others, the continuous adjoint state approach does not require storing intermediate sensitivities. To demonstrate the computational advantage, we consider a domain discretized by 10,000 elements. For each electrode configuration, six adjoint states must be computed (a_φ, a_1 and twice a_0 and a_h). Together with the six forward states (φ_0, h, m_0^c, m_1^c, $m_0^{\varphi'}$, $m_1^{\varphi'}$), the demand of computer memory is limited (12 vectors of 10,000 elements). From this, the three sensitivity vectors $\frac{\partial m_0^{\Delta\varphi'}}{\partial Y}$, $\frac{\partial m_1^{\Delta\varphi'}}{\partial Y}$, $\frac{\partial\left(m_1^{\Delta\varphi'}/m_0^{\Delta\varphi'}\right)}{\partial Y}$ are computed element by element. Using intermediate sensitivities ($\frac{\partial m_k^{\Delta\varphi'}}{\partial m_k^c}$, $\frac{\partial m_k^c}{\partial h}$, $\frac{\partial m_k^c}{\partial Y}$), by contrast, would require evaluating and storing matrices of the size 10,000 × 10,000, without gaining accuracy.

5. Numerical Implementation and Computational Effort

[35] All partial differential equations are solved by the Finite Element Method (FEM) using bilinear, rectangular elements. Hydraulic conductivity is defined as elementwise constant values. For stabilization of advection-dominated transport, we apply the streamline upwind Petrov-Galerkin (SUPG) method [*Brooks and Hughes*, 1982]. *Nowak* [2005] determined analytical expressions for the source terms in the adjoint state equations of temporal moments. By using these, a considerable computational speedup is achieved. The resulting systems of linear equations are solved by a conjugate gradient method with algebraic multigrid preconditioning [*Stüben*, 2001].

[36] Four $n \times n$ matrices (with n being the number of nodes) discretizing partial differential equations must be set up: one for the groundwater flow equation, equation (1), which is self-adjoint, two for solute transport (forward and adjoint), equations (6) and (34), and one for the Poisson equation, equation (18), which is also self-adjoint. In order to evaluate right-hand side vectors from vectors of nodal variables, four more $n \times n$ matrices must be set up, according to equations (25) and (37), equation (28), equation (34), and equation (40), respectively. For a given hydraulic conductivity field and m measurements, evaluating the forward problem and the sensitivities, the groundwater flow equation, equation (1), must be solved with $2m + 1$ right-hand side vectors, the transport equation, equation (25), with $3m + 2$ right-hand side vectors, and the linearized Poisson equation, equation (28), with $2m + 2$ right-hand side vectors, in which we have summed up the number of forward and adjoint problems. For a large number of measurements m, the same systems of linear equations must be solved with multiple right-hand sides. It may thus be recommendable to factorize the systems of equations and use direct solvers instead of iterative ones. These implementational issues, however, are not covered here.

6. Artificial Test

[37] In this section we present an application of the theory outlined in the previous sections to an artificial test case. Although the equations hold also for three spatial dimensions, we simulate a two-dimensional system, to keep computing time and amount of data as low as possible.

6.1. Setup

[38] We simulate an intermediate-scale quasi-two-dimensional sandbox of dimension $L_x \times L_y \times L_z$ with homogeneous filling and therefore uniform hydraulic conductivity K, shown schematically in Figure 1. The domain is discretized by $n_x \times n_z$ elements of size $\Delta x \times \Delta z$. The geometric parameters are listed in Table 1. The top and bottom of the sandbox are no-flow boundaries; along the right and left boundary, the hydraulic head is fixed. This leads to a uniform hydraulic gradient $\partial h/\partial x$ throughout the sandbox. During a specified period of time, t_{inj}, a solution with known tracer concentration c_{in} is injected through the middle part of the boundary z_{in}. Above and below, tracer-

Table 1. Parameters Applied in the Test Case

Parameter	Description	Value
	Geometric Parameters and Discretization	
$L_x \times L_y \times L_z$	length × width × height of domain	3 × 0.05 × 0.6 m
$n_x \times n_z$	number of cells in x and z directions	300 × 60
$\Delta x \times \Delta z$	grid spacings in x and z directions	0.01 × 0.01 m
	Hydraulic Parameters	
$\frac{\partial h}{\partial x}$	hydraulic gradient	0.01
K	hydraulic conductivity	10^{-3} m/s
	Transport Parameters	
θ	porosity	0.4
α_l	longitudinal dispersivity	0.01 m
α_t	transverse dispersivity	0.001 m
D_m	pore diffusion coefficient	10^{-9} m^2/s
	Geoelectrical Parameters	
I	current	2 mA
σ_0	base electrical conductivity	0.03 S/m
κ	linear dependence of electrical conductivity on concentration	0.06 Sm^2/kg
	Boundary Conditions	
c_{in}	concentration in inflow	0.4 g/ℓ
z_{in}	injection height	0.2 0.4 m
	Time Parameters	
t_{inj}	duration of injection	5 h
Δt	time discretization in transient calculation	6 min
t_{meas}	duration of measurement	52 h

free water is injected. The choice of the length of the injection time is important: if a single pulse is injected, the arrival time is very well defined, but the electrical signal is too small to be accurately detected. If the tracer is injected over a longer period of time, we obtain a large signal, but the arrival time is not clearly defined because of the wide spread. Our simulations are carried out for a total injection time of 5 hours, ranging from −2.5 hours to 2.5 hours. Choosing the injection time to be symmetric with respect to time zero causes the first moment of concentration in the inflow to equal zero.

[39] Two rows of electrodes extending through the whole width of the sandbox are situated near the top and bottom boundary. A current is injected and extracted using a pair of electrodes, while the electrical potential is measured at the other electrodes. The presence of the tracer causes a change in electrical conductivity proportional to its concentration (see equation (12)). This consequently causes a perturbation of the electrical potential field in the sandbox (see equation (21)), which is detected by the electrodes and measured at time intervals Δt for a total period of t_{meas}. On the basis of an assumed uniform hydraulic conductivity field throughout the whole domain, we simulated the zeroth and first temporal moments of concentration and of potential perturbation resulting from the tracer injection. For the same setup we computed the sensitivities of the mean arrival time of the electrical signal with respect to the log hydraulic conductivity according to the scheme outlined in section 4. Table 1 lists all parameters for this test case.

6.2. Testing the Validity of Linearization

[40] The main critical assumption of our approach is the validity of linearizing the relationship between perturbations of electrical conductivity and potential (equation (21)). In this section, we want to test under which conditions this assumption is valid.

[41] As a starting point we consider the measured potential difference $\Delta\varphi$ for a given electrode configuration and a uniform electrical conductivity σ:

$$\Delta\varphi = \frac{\alpha I}{\sigma} \tag{47}$$

where α is a proportionality constant. Consequently, if we change the electrical potential uniformly throughout the domain, we obtain the ratio of the measured potential difference with respect to the initial one as

$$\frac{\Delta\varphi(\sigma)}{\Delta\varphi_0} = \frac{\sigma_0}{\sigma} \tag{48}$$

[42] In the linearization of the Poisson equation, we wrote the electrical potential as the sum of the base value plus the variation about it (equation (17)), which can also be expressed as

$$\Delta\varphi_{lin} = \Delta\varphi_0 + \left.\frac{\partial\Delta\varphi}{\partial\sigma}\right|_{\sigma_0} (\sigma \quad \sigma_0) \tag{49}$$

[43] Substituting equation (47) into equation (49) we obtain

$$\frac{\Delta\varphi_{lin}(\sigma)}{\Delta\varphi_0} = 2 \quad \frac{\sigma}{\sigma_0} < 0 \;\forall\; \sigma > 2\sigma_0 \tag{50}$$

[44] For $\sigma = 2\sigma_0$, therefore, the linearization leads to an electrical potential of zero. Further increasing the electrical conductivity would even lead to a negative electrical potential or negative resistivity, which is physically impossible. In the course of a salt tracer test, the electrical conductivity is not increased in a spatially uniform way, so that the effect of linearization is less severe. Nonetheless, linearization will always overestimate the reduction of a potential difference in the time the tracer cloud passes the vicinity of the electrodes.

[45] To show the effects of the linearization we calculated the potential differences through time between two specific electrodes for the linearized and exact cases without normalizing the potentials. In the linearized calculation, the potential perturbation is calculated directly at each time step by equation (21). In the nonlinearized calculation, we have to solve the Poisson equation, equation (13), at each time step and subtract the base potential. The simulations were done using different tracer concentrations, representing different electrical conductivity contrasts with respect to the base value.

[46] Figure 2 shows the change of potential difference through time for a specific electrode configuration (shown in Figure 1) and some selected concentrations (0.1, 0.4, 0.6 and 1 g/ℓ, corresponding to an electrical conductivity contrast of 1.2, 1.8, 2.2 and 3). The smaller the concentration, the better the linearized and nonlinearized curves agree. The problem of using a very low concentration, however, is that the potential differences vary only slightly over time and are therefore difficult to measure accurately. For experimental design, we thus have to find a tradeoff

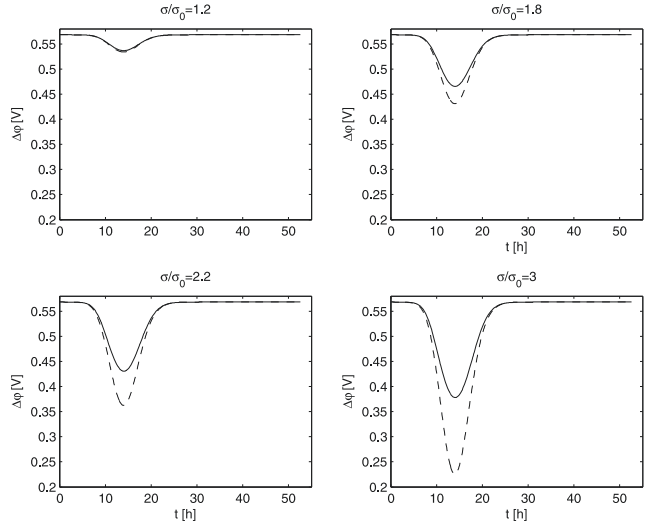

Figure 2. Potential difference as a function of time for different electrical conductivity contrasts, i.e., different input concentrations. Solid line, solution of exact Poisson equation; dashed line, solution of linearized Poisson equation.

between obtaining a sufficiently large signal (requiring high concentrations) and introducing not too large errors by linearization (requiring low concentrations). On the basis of the results shown in Figure 2, we have chosen a concentration of 0.4 g/ℓ (electrical conductivity contrast of 1.8) for the following calculations.

[47] As discussed above, linearizing the Poisson equation about the base electrical conductivity causes a larger deviation of the potential difference from the base value and an overestimation of the zeroth moment of potential perturbation (i.e., the integral under the breakthrough curve), which can be seen in Figure 2. Conversely, the maximum value appears at the same time even for higher tracer concentrations. That is, the ratio of the first over the zeroth moment of potential perturbation, indicating the mean breakthrough time, is correct even in the linearized form of the Poisson equation. The use of the ratio of the temporal moments instead of the zeroth and first moments themselves in further calculations is therefore advantageous, as it minimizes the error due to the linearization. This is also illustrated in Figure 3, which shows the relative error between the linearized and nonlinearized calculation of the moments of potential perturbation as a function of electrical conductivity contrast using the same electrode configuration as before. While the errors for the zeroth and first moment increase approximately linearly with increasing contrast, reaching nearly 60% for a contrast of 3, the linearization has very little effect on the mean arrival time: the maximal error for the chosen concentrations is about 1%.

[48] While Figures 2 and 3 illustrate that the ratio $m_1^{\Delta\varphi'}/m_0^{\Delta\varphi'}$ for the tested electrode configuration is quite accurately approximated by the linearized version of the Poisson equation, these plots do not indicate whether the potential perturbations obtained by the linearized Poisson equation are affected by concentration at the same location as those of the nonlinearized Poisson equation. The latter becomes clearer from the pattern of the direct current streamlines. Because the computation of streamlines is cumbersome in a Finite Element simulation of potentials [e.g., *Cordes and Kinzelbach*, 1992], we consider normalized electrical potentials, $\varphi_{\mathrm{norm}}(\mathbf{x}, t)$ instead:

$$\varphi_{\mathrm{norm}}(\mathbf{x},t) = \frac{\varphi(\mathbf{x},t) \quad \varphi(\mathbf{x_o},t)}{\varphi(\mathbf{x_i},t) \quad \varphi(\mathbf{x_o},t)} \tag{51}$$

in which $\varphi(\mathbf{x}_i, t)$ and $\varphi(\mathbf{x}_o, t)$ are the computed electrical potentials at the current injecting and extracting electrodes, respectively. $\varphi_{\mathrm{norm}}(\mathbf{x}, t)$ ranges between zero and unity, and contour lines of it are perpendicular to direct current streamlines throughout the domain at all times.

[49] At each time step and for each node of the computational grid, the difference between the linearized and exact normalized potential field was calculated. For each point, we computed the maximum absolute difference over time, $\varepsilon_{\max}^{\varphi\mathrm{norm}}(\mathbf{x})$:

$$\varepsilon_{\max}^{\varphi_{\mathrm{norm}}}(\mathbf{x}) = \left\| \varphi_{\mathrm{norm}}^{lin}(\mathbf{x},t) \quad \varphi_{\mathrm{norm}}(\mathbf{x},t) \right\|_{\infty} \tag{52}$$

in which the infinity or maximum norm is taken over the time series.

[50] Figure 4 shows $\varepsilon_{\max}^{\varphi\mathrm{norm}}(\mathbf{x})$ as function of space for the electrode configuration used in all computations so far. Figure 4 also includes the base electrical potential field. For the chosen current electrodes and an electrical conductivity contrast of 1.8, the maximum error in the normalized potential field caused by the linearization is less than 1%. That is, the distortion of the direct current streamlines by the presence of the conductive tracer plume is fairly small. The higher the electrical conductivity contrast, however, the more significant becomes the error. For a contrast of 10, the maximum error reaches already about 50%. That is, a high tracer concentration causes a high electrical conductivity

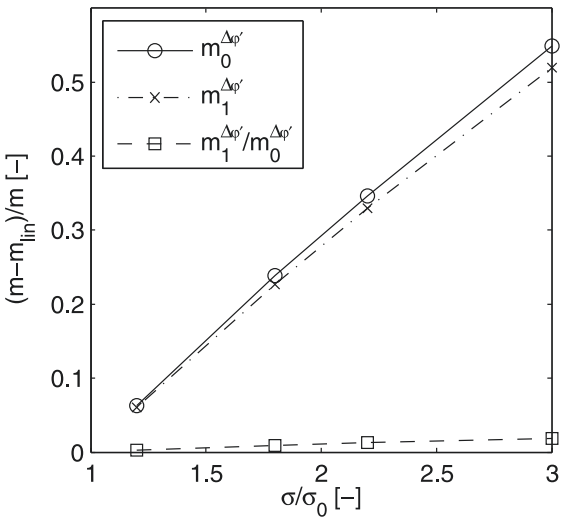

Figure 3. Relative error caused by linearization as a function of electrical conductivity contrast for the zeroth and first moment of potential perturbation and for the mean arrival time of the perturbation; m_{lin} represents the temporal moment on the basis of the linearized Poisson equation.

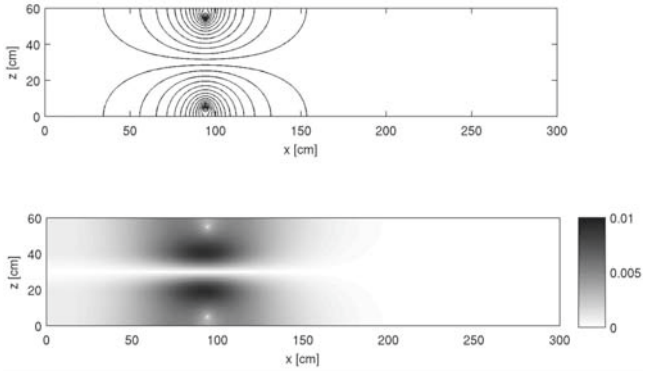

Figure 4. (top) Pattern of the base potential field φ_0 for a pair of current electrodes and (bottom) maximum norm $\varepsilon_{\max}^{\varphi\text{norm}}$ of the differences between the linearized and nonlinearized normalized potential field through time.

contrast and leads to strong distortions of the direct current streamlines. These distortions are neglected in the linearization. We conjecture that too high tracer concentrations would lead to severe errors introduced by using the linearized Poisson equation, implying that the linear temporal moment-generating equations would become significantly biased. The chosen tracer concentration leads to an electrical conductivity contrast of about two which appears to be a reasonable compromise between guaranteeing a well detectable signal and enabling the applicability of the linearized Poisson equation.

[51] The limitations of linearized equations are of course well known in hydrogeological inversion: The groundwater flow equation, equation (1), is formally identical to the Poisson equation, equation (13). A linearized version of the groundwater flow equation can be used only if the variance of log hydraulic conductivity is small; otherwise iterative methods are necessary in the inference of the ln(K) field from head measurements [*Kitanidis*, 1995]. While the contrast in hydraulic conductivity is a given property of the formation under investigation, we can manipulate the contrast in electrical conductivity by choosing the tracer concentration.

[52] The linearization was tested also for other electrode configurations. These configurations are discussed in section 6.4 in the context of sensitivity patterns. With the chosen contrast of 1.8 in electrical conductivity, the linearization caused a relative error in the mean arrival time of the electrical signal smaller than 3% for all tested configurations, and also in an application with a random heterogeneous hydraulic conductivity field.

6.3. Temporal Moments of Concentration and Potential Perturbation

[53] We computed the zeroth and first temporal moments of concentration and potential perturbation for the test case using the moment-generating equations, equations (25) and (28). The results for the moments of concentration, shown in Figure 5, were normalized by the zeroth moment of concentration at the inflow so that the latter equals unity.

[54] The zeroth temporal moment of concentration, m_0^c (Figure 5a) is almost binary: the maximum value is nearly uniform and close to one within the plume, and zero outside. Transverse dispersion slightly smoothes vertical concentration gradients and decreases the maximum value along the center line.

[55] The first moment of concentration, m_1^c, is shown in Figure 5b. Being the zeroth moment multiplied by the mean arrival time, it logically increases with distance from the inflow boundary within the plume. At the edge of the plume, the first moment of concentration exhibits a strong vertical gradient because the zeroth moment does. Outside the plume, m_1^c approaches zero. The ratio of the first over the zeroth moment of concentration, plotted in Figure 5c, also shows a horizontal gradient, with values (indicating travel time in hours) increasing with distance from the inflow boundary. Outside of the main plume, the computed values of m_1^c/m_0^c have no practical relevance, as here the ratio of two very small values is considered.

[56] Figure 6 shows the temporal moments of potential perturbations for a given pair of current electrodes. The spatial patterns of the zeroth (Figure 6a) and first (Figure 6b) moments look rather similar. The largest effects are obtained near the current electrodes, while a significant part of the domain is hardly affected by the injected current, and thus changes in electrical conductivity caused by the tracer test have no effect either. Near the electrodes, the pattern of the first moment of potential perturbation (Figure 6b) is slightly shifted to the right in comparison to the zeroth moment (Figure 6a). This is so because the first moment of concentration increases with travel distance.

[57] Figure 6c shows the ratio of the first over the zeroth moment of potential perturbations for the same current electrode pair used before. We again observe an increase with travel distance, but the pattern is deformed by the location of the electrodes and by the area affected by the tracer plume.

6.4. Sensitivities

[58] We computed the sensitivities of the temporal moments of potential perturbation with respect to log hydraulic conductivity as described in section 4. The sensitivities quantify the effect of a slight increase or decrease in hydraulic conductivity at a specific point of the domain on the temporal moments of potential perturbation. By this analysis, we can identify which parts of the domain affect the measurements. Figure 7 shows the results for the same electrode configuration used in section 6.2. As shown in Figures 7a and 7b, the highest sensitivities for the zeroth and first moment of potential perturbation with respect to log hydraulic conductivity are found in the regions with the highest concentration gradients (at the edge of the tracer plume) and where the gradients of the electrical potential or its adjoint state are highest (near the electrodes). The high sensitivities in the zones of high gradients can be explained by equation (40), where the gradient of the temporal moments of concentration appears as a source-sink term. Equation (34) shows the influence of the gradients of electrical potential and its adjoint state on the adjoint state of the first moment of concentration and consequently also on the sensitivity with respect to the hydraulic conductivity field. Because the gradients of electrical potential are highest near the current electrodes, and that of its adjoint state near the potential electrodes, varying the electrode configuration changes the sensitivity patterns (see below).

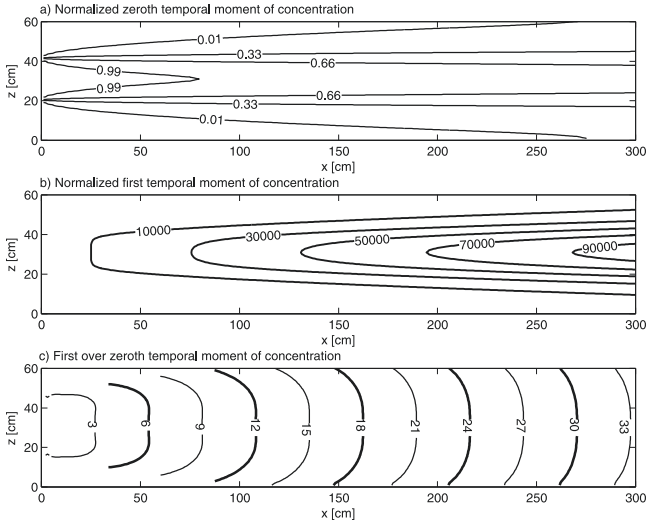

Figure 5. Normalized temporal moments of concentration: (a) zeroth moment, m_0^c, (b) first moment, m_1^c, and (c) ratio of the two (arrival time in hours) for the given example.

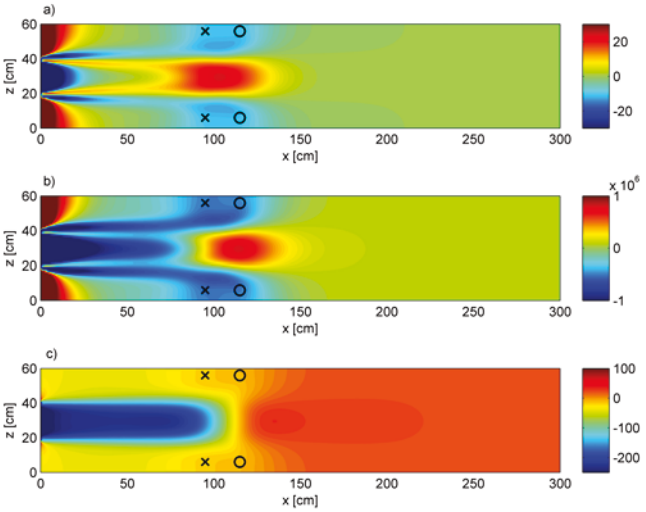

Figure 7. Sensitivities of (a) zeroth, (b) first, and (c) first over zeroth moments of potential perturbation, $m_1^{\Delta\varphi'}/m_0^{\Delta\varphi'}$, with respect to log hydraulic conductivity. Crosses, positions of the current electrodes; circles, positions of the potential electrodes.

[59] In the present application, the hydraulic conductivity distribution is assumed uniform throughout the sandbox. A nonuniform hydraulic conductivity field would change the velocity field and the spatial pattern of the temporal moments of concentration. The latter would also influence the sensitivity pattern. That is, the sensitivity fields of electrical potential moments depend on the hydraulic conductivity distribution in the domain. This implies that an inverse model, in which the hydraulic conductivity field is inferred from measurements of electrical potential moments, must be iterative.

[60] Figure 7c shows the sensitivity of the ratio of the first over the zeroth temporal moment (mean arrival time) of potential perturbation with respect to log hydraulic conductivity. Here we notice a negative sensitivity in the tracer plume upstream of the electrodes. This means that an increase in the hydraulic conductivity in the region through which the tracer is transported, leads to a decrease in the ratio of the first over the zeroth temporal moment of potential perturbation, which represents an earlier arrival time of the tracer in the measurement area. This is to be expected, as the flow is faster because of the increase of hydraulic conductivity. Figure 8 shows the sensitivities of $m_1^{\Delta\varphi'}/m_0^{\Delta\varphi'}$ with respect to the log hydraulic conductivity for the same current and potential electrode geometry, but shifted in the longitudinal direction of the sandbox. The high negative sensitivities clearly follow the tracer path, but only to about the location of the electrodes. This type of

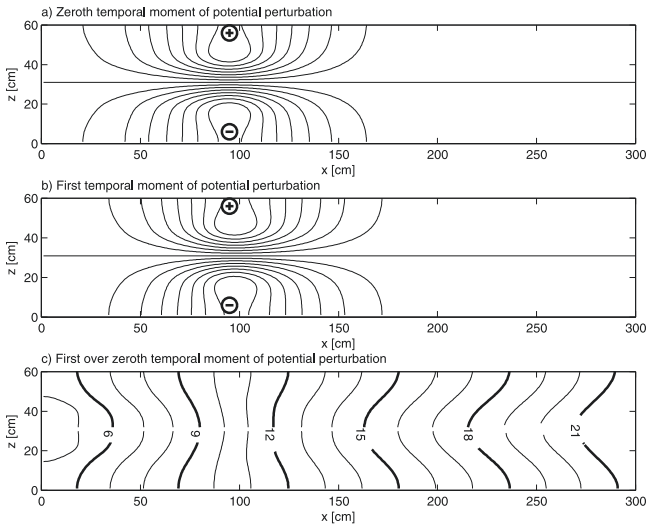

Figure 6. Temporal moments of potential perturbation: (a) zeroth moment, $m_0^{\varphi'}$, (b) first temporal moment, $m_1^{\varphi'}$, and (c) ratio of the two (arrival time in hours) for the given example.

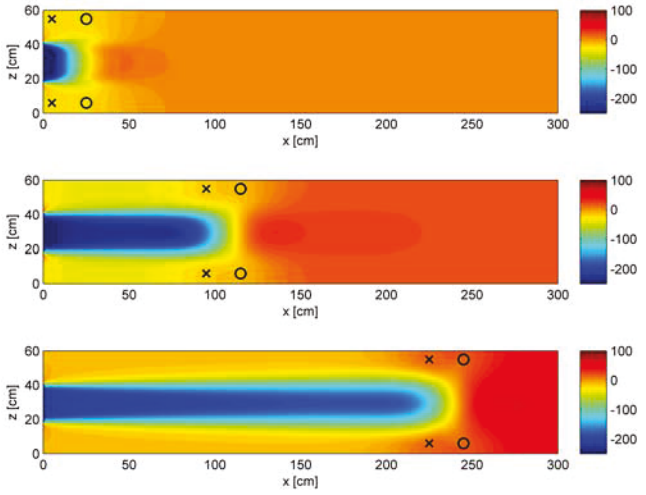

Figure 8. Sensitivity of first over zeroth moment of potential perturbation, $m_1^{\Delta\varphi'}/m_0^{\Delta\varphi'}$, for three different electrode locations. Crosses, positions of the current electrodes; circles, positions of the potential electrodes.

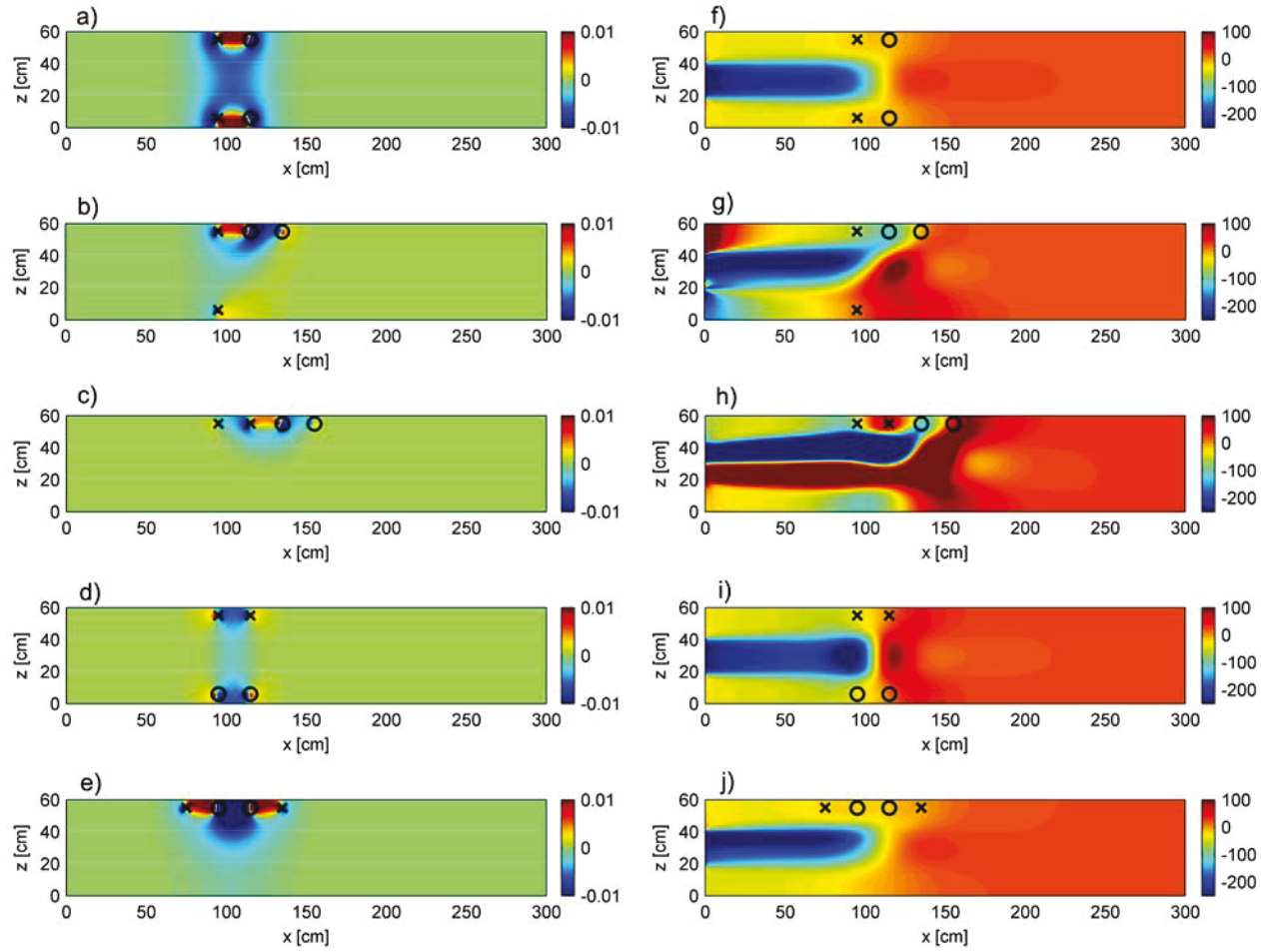

Figure 9. (left) Sensitivity of electrical potential, $\Delta\varphi'$, with respect to tracer concentration c for five different electrode configurations. White lines, boundaries of the tracer plumes neglecting transverse dispersion. (right) Sensitivity of first over zeroth moment of potential perturbation, $m_1^{\Delta\varphi'}/m_0^{\Delta\varphi'}$, with respect to log hydraulic conductivity for the same electrode configurations as in the left plots. Crosses, positions of the current electrodes; circles, positions of the potential electrodes.

sensitivity pattern is already known from direct point-like measurements of concentrations analyzed by the mean arrival time [*Cirpka and Kitanidis*, 2000; *Nowak*, 2005].

[61] The same calculations were also done for selected other electrode configurations (i.e., different geometries), in order to view the differences in the sensitivity pattern caused by changing the relative position of the current and potential electrodes. Figure 9 shows the sensitivities of the electrical potential with respect to the tracer concentration (which is proportional to the electrical conductivity) and the sensitivities of the mean arrival time of the potential perturbation with respect to the log hydraulic conductivity for some selected electrode configurations. The sensitivity density of the electrical potential with respect to concentration is identical to the source-sink term on the right-hand side of equation (34). This quantity is shown in the left column of Figure 9, and represents the source-sink term for calculating the adjoint state of the first moment of potential perturbation. It can be interpreted as the measurement function of concentration. For a point-like measurement of concentration, as obtained by an in situ probe, the sensitivity of the mean arrival time with respect to log hydraulic conductivity is mainly a narrow stripe in upstream direction [*Cirpka and Kitanidis*, 2000; *Nowak*, 2005]. With the ERT survey, a spatially distributed measurement of concentration is implemented. This results in a sensitivity pattern with respect to log hydraulic conductivity that may be constructed by integrating the sensitivities of point-like measurements weighted by the measurement function at a given location. As the injection of the tracer was restricted to the central part of the sandbox, the sensitivities of electrical potential with respect to concentration outside the plume do not influence the sensitivity pattern for the arrival time of potential perturbation with respect to log hydraulic conductivity. In Figures 9a, 9b, 9c, 9d, and 9e, the approximate boundary of the plume is indicated by a white line. For the reason discussed above, the sensitivity patterns in Figures 9f, 9i and 9j differ only slightly. In all of these cases, the sensitivity of the potential measurements with respect to concentration is negative within the plume, leading to a more or less uniform negative sensitivity of $m_1^{\Delta\varphi'}/m_0^{\Delta\varphi'}$ with respect to $\ln(K)$ within the plume upstream of the electrodes. The only tested pattern which is significantly different from the one shown in Figure 9f is the dipole-dipole configura-

tion (Figure 9h), which is sensitive only to electrical conductivity at the top half of the domain. The change of sign in the sensitivity of the electrical potential with respect to concentration, in conjunction with the tracer being transported mainly along a certain corridor, leads to an intricate sensitivity pattern of the arrival time of potential perturbation with respect to log hydraulic conductivity. A larger distance of the two dipoles would lead to a deeper penetration of the sensitivity of potentials with respect to concentration which in turn would change the sensitivity pattern with respect to log hydraulic conductivity.

[62] In an optimal experimental design, configurations are chosen which are the least correlated to each other, so that redundancy is minimized. For a limited number of configurations, we would suggest combining measurements that are sensitive over the entire width of the plume, such as the one chosen in Figure 9f, with those that are more sensitive at one side, such as the one chosen in Figure 9h and its symmetric counterpart, and moving these arrays along the whole length of the domain.

7. Conclusions

[63] In the current study, we have shown that temporal moments of electrical potential perturbations are suitable condensates to be used in geoelectrical monitoring of salt tracer tests. We have presented temporal moment-generating equations, relating the measured quantities to hydraulic conductivity in a rigorous fashion. The only approximation lies in linearizing the Poisson equation about the base conductivity. We could show that this approximation is acceptable when the tracer concentration is carefully chosen and when the ratio of first over zeroth temporal moment of potential perturbation is taken as primary measurement.

[64] We have extended the approach of using temporal moments of concentration measurements used in previous studies by adding the measurement equations applicable for geoelectrical monitoring. The advantages of using temporal moments remain: (1) the amount of measured data is condensed without losing too much information, (2) the forward equations consist of a series of steady state equations, reducing the computational effort, and (3) sensitivities can also be computed by a series of steady state adjoint equations.

[65] We could show that the sensitivity patterns are meaningful. Increasing the hydraulic conductivity within the plume at a location upstream of the electrodes decreases the time to pass until the signal is detected by geoelectrical surveying. In comparison to point-like measurements of concentration, the sensitivity pattern for ERT surveys is much more spread, which results from the sensitivity of potentials on concentration. This already implies limitations of the method, because it will be difficult if not impossible to identify fine-scale hydraulic features.

[66] As in all simulations of processes described by partial differential equations, boundary conditions may have a major impact on the solution. Our virtual test case was aimed to mimic a sandbox experiment which is currently in its design phase. This particular application is truly two dimensional, and all boundaries are electrically insulated. Tracer tests in the field would be three dimensional, and electrical insulation would be guaranteed only at the land surface. In order to minimize artifacts by erroneous boundary conditions, it is thus important to differentiate between boundaries for the flow-and-transport problem and for the direct current (DC) problem. The domain for the DC problem may be chosen larger, and the electrical properties of an underlying aquitard must be accounted for in the simulation.

[67] We have presented all ingredients necessary for hydrogeophysical inversion of salt tracer experiments in groundwater, with the exception of the inverse kernel. We plan to implement the presented approaches of calculating the temporal moments of electrical potential perturbation and their sensitivity with respect to hydraulic conductivity in the quasi-linear geostatistical inverse method used for hydraulic measurements [*Kitanidis*, 1995]. The approaches presented in this paper, however, could also be combined with any other inversion scheme for distributed parameter fields.

[68] **Acknowledgments.** We thank Kamini Singha, two anonymous reviewers, and the associate editor, Lee Slater, for their constructive remarks in helping to improve the quality of the paper. This research is part of the RECORD project of the Competence Center Environment and Sustainability (CCES) within the ETH domain. Funding has been provided by the Swiss National Science Foundation under grant 200021-113296.

References

Archie, G. E. (1942), The electrical resistivity log as an aid in determining some reservoir characteristics, *Tech. Rep. 1422*, Am. Inst. Min. Metall. Pet. Eng., New York.

Binley, A., S. Henry-Poulter, and B. Shaw (1996), Examination of solute transport in an undisturbed soil column using electrical resistance tomography, *Water Resour. Res.*, *32*(4), 763 769.

Binley, A., G. Cassiani, R. Middleton, and P. Winship (2002), Vadose zone flow model parameterisation using cross-borehole radar and resistivity imaging, *J. Hydrol.*, *267*(3 4), 147 159.

Brooks, A. N., and T. J. R. Hughes (1982), Streamline upwind/Petrov-Galerkin formulations for convection dominated flows with particular emphasis on the incompressible Navier-Stokes equations, *Comput. Methods Appl. Eng.*, *32*(1 3), 199 259.

Cirpka, O. A., and P. K. Kitanidis (2000), Sensitivity of temporal moments calculated by the adjoint-state method and joint inversing of head and tracer data, *Adv. Water Resour.*, *24*(1), 89 103.

Cordes, C., and W. Kinzelbach (1992), Continuous groundwater velocity fields and path lines in linear, bilinear, and trilinear finite elements, *Water Resour. Res.*, *28*(11), 2903 2911.

Daily, W., A. Ramirez, D. LaBrecque, and J. Nitao (1992), Electrical resistivity tomography of vadose water movements, *Water Resour. Res.*, *28*(5), 1429 1442.

Day-Lewis, F. D., and K. Singha (2008), Geoelectrical inference of mass transfer parameters using temporal moments, *Water Resour. Res.*, *44*, W05201, doi:10.1029/2007WR006750.

Dey, A., and H. F. Morrison (1979), Resistivity modelling for arbitrarily shaped two-dimensional structures, *Geophys. Prospect.*, *27*, 106 136.

Harvey, C. F., and S. M. Gorelick (1995), Temporal moment-generating equations: Modeling transport and mass transfer in heterogeneous aquifers, *Water Resour. Res.*, *31*(8), 1895 1911.

James, A. I., W. D. Graham, K. Hatfield, P. S. C. Rao, and M. D. Annable (2000), Estimation of spatially variable residual nonaqueous phase liquid saturations in nonuniform flow fields using partitioning tracer data, *Water Resour. Res.*, *36*(4), 999 1012.

Jose, S. C., and O. A. Cirpka (2004), Measurement of mixing-controlled reactive transport in homogeneous porous media and its prediction from conservative tracer test data, *Environ. Sci. Technol.*, *38*(7), 2089 2096.

Kemna, A., J. Vanderborght, B. Kulessa, and H. Vereecken (2002), Imaging and characterisation of subsurface solute transport using electrical resistivity tomography (ERT) and equivalent transport models, *J. Hydrol.*, *267*(3 4), 125 146.

Kitanidis, P. K. (1995), Quasi-linear geostatistical theory for inversing, *Water Resour. Res.*, *31*(10), 2411 2419.

Li, W., W. Nowak, and O. A. Cirpka (2005), Geostatistical inverse modeling of transient pumping tests using temporal moments of drawdown, *Water Resour. Res.*, *41*, W08403, doi:10.1029/2004WR003874.

Li, W., A. Englert, O. A. Cirpka, J. Vanderborght, and H. Vereecken (2007), Two-dimensional characterization of hydraulic heterogeneity by multiple pumping tests, *Water Resour. Res.*, *43*, W04433, doi:10.1029/2006WR005333.

Li, W., A. Englert, O. A. Cirpka, and H. Vereecken (2008), Three-dimensional geostatistical inversion of flowmeter and pumping-test data, *Ground Water*, *46*(2), 193 201, doi:10.1111/j.1745-6584.2007.00419.x.

Nowak, W. (2005), Geostatistical methods for the identification of flow and transport parameters in the subsurface, Ph.D. thesis, Inst. fuer Wasserbau, Univ. Stuttgart, Stuttgart, Germany.

Nowak, W., and O. A. Cirpka (2006), Geostatistical inference of hydraulic conductivity and dispersivities from hydraulic heads and tracer data, *Water Resour. Res.*, *42*, W08416, doi:10.1029/2005WR004832.

Rizzo, E., B. Suski, A. Revil, S. Straface, and S. Troisi (2004), Self-potential signals associated with pumping tests experiments, *J. Geophys. Res.*, *109*, B10203, doi:10.1029/2004JB003049.

Rubin, Y., and S. S. Hubbard (2005), *Hydrogeophysics*, *Water Sci. Technol. Libr.*, vol. 50, Springer, Dordrecht, Netherlands.

Singha, K., and S. M. Gorelick (2005), Saline tracer visualized with three-dimensional electrical resistivity tomography: Field-scale spatial moment analysis, *Water Resour. Res.*, *41*, W05023, doi:10.1029/2004WR003460.

Singha, K., F. D. Day-Lewis, and J. W. Lane, Jr. (2007), Geoelectrical evidence of bicontinuum transport in groundwater, *Geophys. Res. Lett.*, *34*, L12401, doi:10.1029/2007GL030019.

Slater, L. (2007), Near surface electrical characterization of hydraulic conductivity: From petrophysical properties to aquifer geometries A review, *Surv. Geophys.*, *28*, 169 197, doi:10.1007/s10712-007-9022-y.

Slater, L., A. M. Binley, W. Daily, and R. Johnson (2000), Cross-hole electrical imaging of a controlled saline tracer injection, *J. Appl. Geophys.*, *44*(2 3), 85 102.

Sloan, S. D., G. P. Tsoflias, and D. W. Steeples (2007), Shallow seismic AVO variations related to partial water saturation during a pumping test, *Geophys. Res. Lett.*, *34*, L22405, doi:10.1029/2007GL031556.

Stüben, K. (2001), A review of algebraic multigrid, *J. Comput. Appl. Math.*, *128*(1 2), 281 309.

Sun, N. Z., and W. W.-G. Yeh (1990), Coupled inverse problems in groundwater modeling: 1. Sensitivity analysis and parameter identification, *Water Resour. Res.*, *26*(10), 2507 2525.

Vanderborght, J., A. Kemna, H. Hardelauf, and H. Vereecken (2005), Potential of electrical resistivity tomography to infer aquifer transport characteristics from tracer studies: A synthetic case study, *Water Resour. Res.*, *41*, W06013, doi:10.1029/2004WR003774.

O. A. Cirpka, Center of Applied Geosciences, University of Tübingen, Sigwartstrasse 10, D-72076 Tübingen, Germany. (olaf.cirpka@uni-tuebingen.de)

D. Pollock, Eawag, Swiss Federal Institute of Aquatic Science and Technology, Überlandstrasse 133, CH-8600 Dübendorf, Switzerland. (davina.pollock@eawag.ch)